Subproject A1.6

Tunable Photonic Metamaterials

Principle Investigators: Lihua Shao, Matthias Ruther, Stefan Linden, Martin Wegener, Jörg Weissmüller

CFN-Financed Scientists: Lihua Shao (3/4 BAT IIa, 12 months)

Further Scientists:

Institut für Nanotechnologie
Forschungszentrum Karlsruhe in der Helmholtz-Gemeinschaft

Tunable Photonic Metamaterials

Introduction and Summary

Nanomaterials with tunable electronic structure exploit the large specific surface area of metal nanostructures along with the strategy of tuning the surface properties through the controlled introduction of space-charge regions for creating materials with tunable macroscopic properties [1,2]. Photonic metamaterials provide an unconventional optical response – in the extreme, negative refractive indices – by lithographically structured elements such as arrays of split-ring resonators (SRR) [3]. Work in Project A1.06 aims at combining these two materials design strategies into a photonic metamaterial in which the space-charge at the surface of each SRR is controlled via an applied potential. Since the space charge couples into the electric resistivity, the resonance frequency of the metamaterials as well as the damping would be reversibly shifted. Our research – done in close cooperation with A1.05 – indeed confirms that concept, exemplifying the new opportunities for designing functional nanomaterials which exploit nanoscale structure along with interfacial processes at electrode surfaces. Furthermore, the combination of lithographic structuring with electrochemical cycling has lead to a qualitative progress in metamaterial processing. This report summarizes the results on both topics, as published in Refs. [4] and [5].

1. Experiment procedures

In our electrochemical experiments, we employ gold nanoantennae arrays [5] and arrays of gold split-ring resonators [6] (SRR). Each array has a footprint of 80 μm × 80 μm. An example of a 10-nm thin gold structure is shown in the inset in Fig. 1(a). The nanoantennae and the SRR arrays have been fabricated using a lift-off procedure following standard electron-beam lithography [6] on glass substrates coated with a 10-nm thin film of indium tin oxide (ITO) and a 2 to 3-nm thin Cr film as adhesion promoter. Additional results (not shown here) were obtained with a series of samples deposited without the Cr layer. These samples tended to detach after repeated electrochemical cycles, but results were otherwise consistent with those obtained with the Cr layer. All films (ITO, Cr, and Au) are made using high-vacuum electron-beam deposition. Gold is deposited at a rate of 0.1 nm/s. The average film thicknesses are determined by atomic-force microscopy (AFM). The ITO provides the contact to the gold nanostructures, which form the working electrode in our electro-modulation experiments.

The electrochemical cell is a quartz glass cuvette filled with a 0.7 M solution of NaF (Suprapur, Merck) in ultrapure 18.2 MΩ cm grade water (Arium 611, Sartorius) and open to air. Cleaning procedures are analogous to Ref. [7]. The metamaterial sample is immersed in the solution and its potential – as measured relative to a standard reference electrode (RE), Ag/AgCl in saturated KCl solution – is controlled by a commercial potentiostat (VoltaLab PST 050, Radiometer Analytical). In this fashion we can reproducibly control the electrode potential and specify its value at an absolute scale. The RE has negligible leakage, preventing Cl^- contamination of the main cell. Optical spectra were recorded at constant potential, after the decay of the initial charging current transient. We use a macroscopic gold spiral as the counter electrode within the electrolyte. The aqueous electrolyte is opaque in the near-infrared (i.e., for wavelengths larger than 1.4 μm, equivalent to frequencies below 214 THz). Hence, we have chosen the SRR sizes such that the resonances of interest lie in the near-infrared part of the electromagnetic spectrum. This leads to SRR side lengths on the order of 100 nm (see inset in Fig. 1(a)).

2. Electrochemical Restructuring of Plasmonic Metamaterials

The electrochemical processes at the gold surface under the conditions of our experiment can be identified based on the cyclic voltammograms of current versus potential, U, during cyclic scans of U (Fig. 1(a)). The most distinctive feature is a peak at positive potential that occurs only during the first scan. This peak is absent if no Cr adhesion layer is used (not depicted). Thus, the peak can be linked to partial dissolution of Cr. In the subsequent cycles, peaks in the potential range $U > 0$ correspond to the reversible adsorption and desorption of oxygen species not exceeding one adsorbed monolayer. We estimate a corresponding variation of the surface charge density of 1.7 electron per surface gold atom, consistent with literature [8]. The large current values at $U < 0$ indicate Faraday reactions related to oxygen trace contaminants in the open cell.

Extinction spectra are shown in Fig. 1(b). As usual, the extinction is defined as the negative logarithm of the intensity transmittance, i.e., unity extinction corresponds to a suppression of the transmittance by one order of magnitude. In these experiments, the full opening angle of the cone of light is 5 degrees, approximating very nearly normal-incidence conditions. Normalization of the transmittance spectra is with respect to the bare ITO-coated substrate, i.e., without the Cr/Au nanostructures, in the same electrochemical cell (5 mm electrolyte thickness). In this fashion, the optical properties of the electrochemical cell drop out. The transmittance of the entire electrochemical cell is about 50 % (not shown). This means that the electrolyte absorption does not significantly affect the plasmonic damping. After completion of sample fabrication, the 10-nm thin gold structures show only a very broad plasmonic resonance – in air as well as in the electrolyte. This is not surprising in view of the very large gold electron scattering/damping due to the considerable surface roughness and presence of grain boundaries expected for such very thin evaporated amorphous gold films. However, after 10 electrochemical cycles over a range from - 0.9 V to +1.3 V – which we will call the “training” phase in what follows – a much more pronounced and sharper plasmonic resonance appears (for thicker gold films, the plasmonic resonances exhibit low damping even without initial electrochemical cycling [6]). This extinction resonance centered at around 300 THz frequency in Fig. 1(b) corresponds to a higher-order resonance of the SRR that can be excited for vertical incident linear polarization of light [6]. The measured extinction spectra can be well fitted by Lorentzians, providing us with the resonance position (±0.5 THz) and the resonance half-width-at-half-maximum (or damping). In Fig. 1(b), the extracted damping reduces from more than 100 THz to 27 THz. This training effect clearly correlates with the change in the cyclic voltammogram after the first complete cycle and it is only observed if the scan includes potentials $U > 0.9$ V.

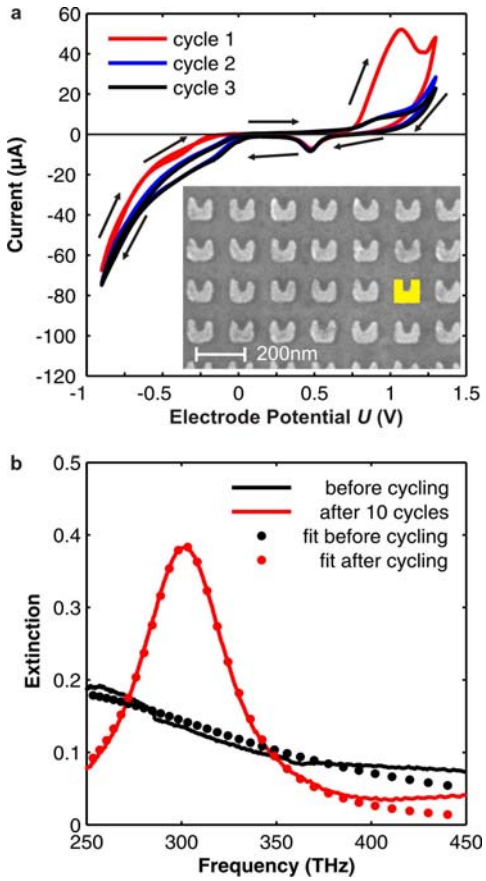

Fig. 1 a) Typical cyclic voltammograms of an array of 10-nm thin gold split-ring resonators (scanning electron micrograph shown as inset) in a NaF-based aqueous electrolyte for electrode potentials ranging from –0.9 to +1.3 V. The first cycle is shown in red, the second in blue, and the third in black. Further cycles coincide within the linewidth of the curves. b) Corresponding normal-incidence extinction spectra for vertical incident linear polarization of light and for open-circuit conditions before (black symbol) and after N=10 complete cycles (red symbol). The solid curves represent Lorentzian fits to the measured data. Note the very substantial sharpening of the resonance.

In the following, we systematically investigate this training aspect in terms of a postprocessing procedure that reduces the plasmonic losses under ambient conditions after electrochemical processing. Arrays composed of rectangular gold pads (antennas) serve as an example. We observe huge effects for film thicknesses near the percolation threshold and significant effects for typical gold-film thicknesses on the order of 20–30 nm. Any such postprocessing is mainly expected to reduce excessive Ohmic (or nonradiative) damping. Small effects on the radiative damping may arise though due to changes in the metal nanostructure shape. Ideally, after postprocessing, one is left with the intrinsic radiative damping only.

The resulting Lorentzians fit parameters (during cycling within the electrolyte), i.e., the damping and the resonance center frequency, are depicted in Fig. 2. Clearly, the damping gradually decreases and the center frequency gradually shifts toward the blue. This effect can be phenomenologically explained by a decrease in the resistance and capacitance of the gold nanostructures due to surface restructuring. Superimposed on these trends, we find electrochemical modulation of the transmittance within each cycle, which we will depict in the next section. In terms of an electrochemical postprocessing procedure, the comparison of the corresponding extinction spectra in air (rather than in the electrolyte) before and after the complete cycling is relevant.

Corresponding data are exhibited in the right column of Fig. 3 for the two orthogonal linear incident polarizations of light and for five different gold-film thicknesses (a)–(e). In each of these cases, we find a substantial sharpening of the plasmonic resonances. As expected for any harmonic-oscillator resonance, this sharpening due to loss reduction is accompanied by an increase in the extinction peak height.

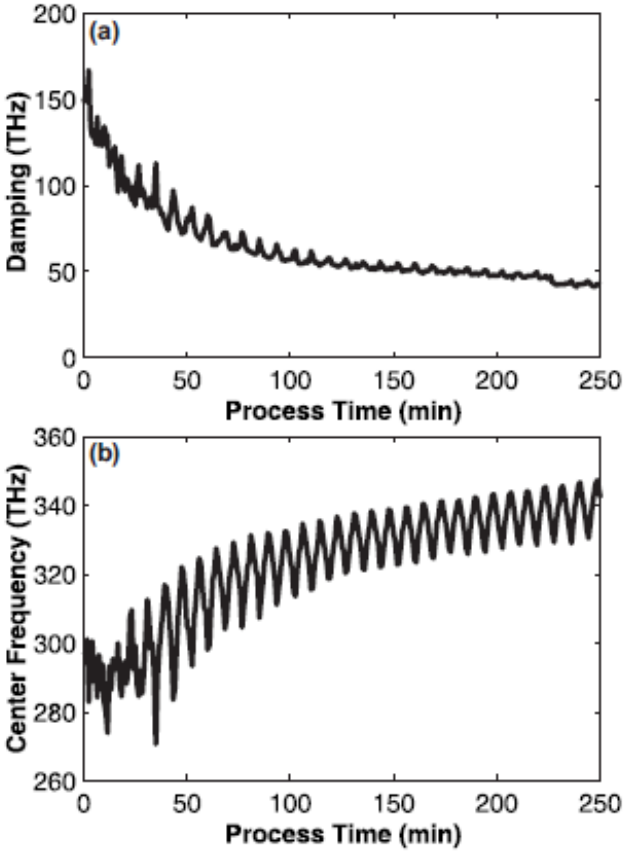

Fig. 2. (a) Plasmonic damping and (b) resonance center frequency vs. time as derived from Lorentzian fits to the measured extinction spectra taken under normal incidence with horizontal polarized light inside the electrolyte during periodic electrochemical cycling in the potential window from –0.9 to +1.0 V and a cycling time of about 8 min/cycle. Note the beneficial reduction in damping (i.e., losses) vs. time. The sample in this example is an array of gold pads with dimensions 145×95 nm^2, a lattice constant of 300 nm, and an average gold-film thickness of 7.9 nm.

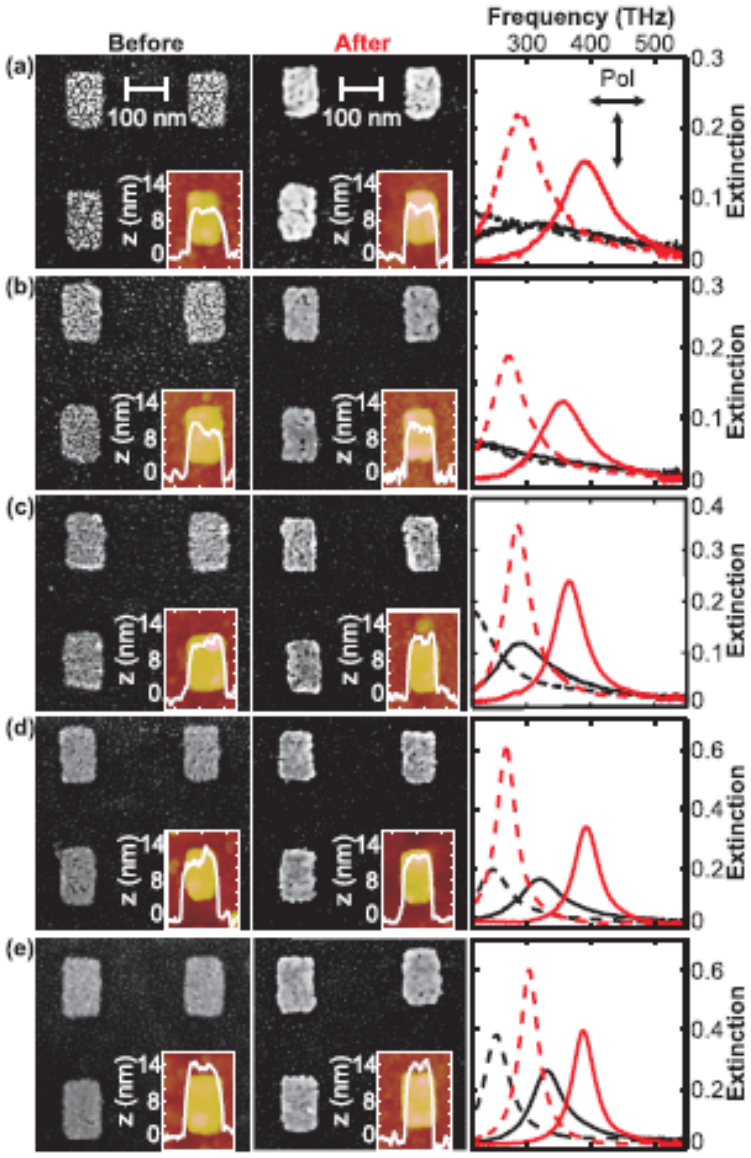

Fig. 3. (Color) Gold nanoantennae arrays of different average gold-film thicknesses [increasing from (a) to (e) with 7.1, 7.9, 8.6, 9.8, and 11.5 nm] before and after electrochemical cycling (see Fig. 2). All data are taken under ambient conditions, i.e., outside of the electrolyte. The left column exhibits electron micrographs before cycling as well as AFM data on one antenna with an AFM line scan profile. The center column depicts corresponding data after cycling. Note the distinct changes in the spectra that are especially pronounced for thin gold structures. The right column reveals corresponding measured normal-incidence extinction spectra before (black curves) and after (red curves) cycling for vertical (dashed) and horizontal (solid) incident linear polarizations of light.

It is interesting to ask whether these beneficial optical trends are accompanied by signatures in the electron micrographs and/or AFM images before (left column of Fig. 3) and after (center column) the complete electrochemical cycling. To allow for a direct comparison and to obtain good image contrast, we have adjusted the gray levels in the electron micrographs such that the substrate on average appears black, whereas the gold antennae on average appear white. The resulting effects in Fig. 3 are most pronounced for thin "films" near or even below the percolation threshold. For example, for a nominal gold-film thickness of 7.1 nm, the disconnected islands of gold "before" cycling develop into a film "after" the cycling. This trend is also accompanied by a slight reduction

in the lateral extent of the metal pads. In contrast, the gold thickness as observed in the AFM data hardly changes between before and after. To emphasize this aspect, we show an AFM line scan through the center of the pad in each case. Note that the films after cycling appear much smoother in the scanning electron microscopy image. The AFM tip is obviously not able to reach into the steep valleys seen in the electron micrographs (because of its large opening angle). It has been reported that transient roughening, accompanied by an increase in surface diffusivity, accompanies the oxidation/reduction treatment of noble metal electrodes [9, 10]. In our experiments, the "smoothening" also only happened when we included an oxidation/reduction potential window, and from the Lippmann equation it is known that in this potential window the gold-electrolyte surface tension is reduced [11]. The reduction in the surface tension of the gold-electrolyte interface favors wetting of the substrate by gold and, therefore, a smoother surface. We conclude that the change in the optical properties is accompanied by a clear restructuring of the gold atoms within the antennae that is most pronounced for very thin films. The training effect also reproducibly persists once the nanostructure is removed from the electrolyte, making it useful as a simple electrochemical post-processing step for metamaterial fabrication. This approach complements recent work in a different size and thickness regime based on thermal annealing [12].

3. Electrochemical Modulation of Photonic Metamaterials

Once the plasmonic resonance is established by electrochemical training, it also persists within the electrolyte, allowing for further studies. The resulting extinction spectra for one complete cycle and for a rather large electrode-potential window ranging from –0.9 V to + 1.3 V are shown in Fig. 4(a). Obviously, the resonance exhibits a substantial red shift with respect to zero bias for positive potentials and a blue shift for negative potentials. Altogether, the peak of the extinction spectrum shifts by as much as 55 THz within one cycle, which is about 18% of the center frequency or more than twice the damping for zero electrode potential (24 THz). For example, the reduction of the extinction spectrum peak of 0.42 (at 50 mV) to 0.14 (at 1300 mV) at 318 THz frequency corresponds to a change of the transmittance from 38% to 72%, i.e., a change of transmittance by about a factor of two. In addition to this shift, the resonance damping also varies with potential. It increases from 24 THz at U = 0.05 V to 31 THz at U = + 1.3 V and to 36 THz at U = −0.9 V. Further extinction data for two complete cycles are shown as a false-color plot in Fig. 4(b).

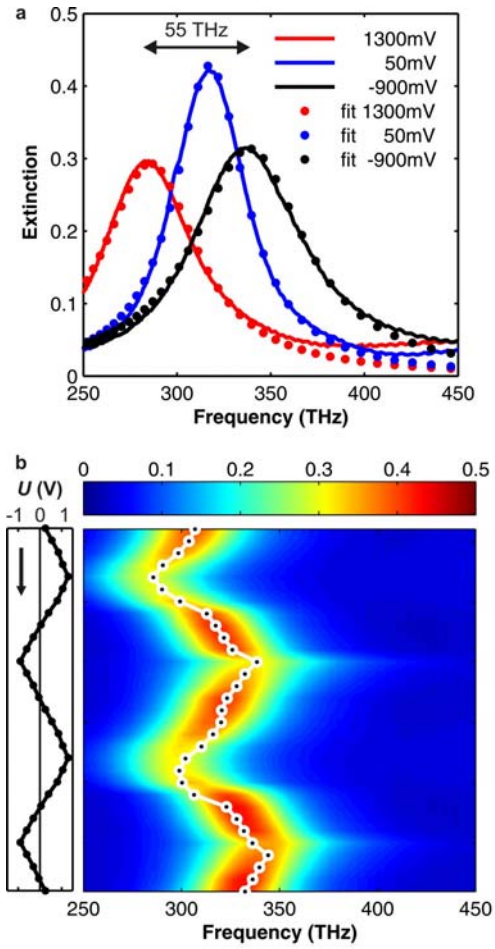

Fig. 4. The electrode potential is varied in a window ranging from –0.9 to □□1.3 V (compare Fig. 1 a)). a) Three selected extinction spectra from one electrochemical cycle taken after N=10 training cycles. The solid curves are Lorentzian fits to the data, the observed peak-to-peak frequency shift of 55 THz is indicated. b) Further extinction spectra plotted on a false-color scale for two complete electrochemical cycles (2 hours acquisition time, time runs from top to bottom) under the same conditions as a). The electrode potential varies as shown on the left-hand side; the dots correspond to the actually measured values. The white dots in the false-color plot indicate the resonance center frequencies as obtained from the Lorentzian fits.

While the modulation of the gold surface-charge density is expected to be a reversible effect, the electrochemical training as described above is clearly irreversible. It is also obvious from Fig. 4(b) that the resonance position after two cycles does not quite recover its original position. This raises the question what fraction of the 55-THz frequency shift in Fig. 4(a) is reversible and what fraction is irreversible. To address this important question, we cycle the electrode potential several times for two smaller electrode-potential windows while observing the extinction spectra for similar samples. The resulting resonance positions (as extracted from the Lorentzian fitting) are summarized in the left-hand side column of Fig. 5, the dampings in the right-hand side column. Following the above 10-cycles training procedure, we start with the small electrode-potential window ranging from –0.5 V to +0.9 V shown in Fig. 5(a). The three depicted complete cycles reveal little if any irreversible effect. Next, the electrode-potential window is increased from –0.9 V to +0.9 V in F Fig. 5(b). Obviously, the modulation becomes somewhat hysteretic and exhibits a drift towards higher frequencies, i.e., the resonance does not quite come back to the same position after one cycle. However, this irreversible part essentially saturates after another 100 cycles under the same conditions as shown in Fig. 5(c). Here, we obtain reversible frequency shifts as large as 25 THz–

which is still comparable to the resonance damping for zero electrode potential (35 THz for this sample). We assign the irreversible contributions to structural changes similar to those during the initial training.

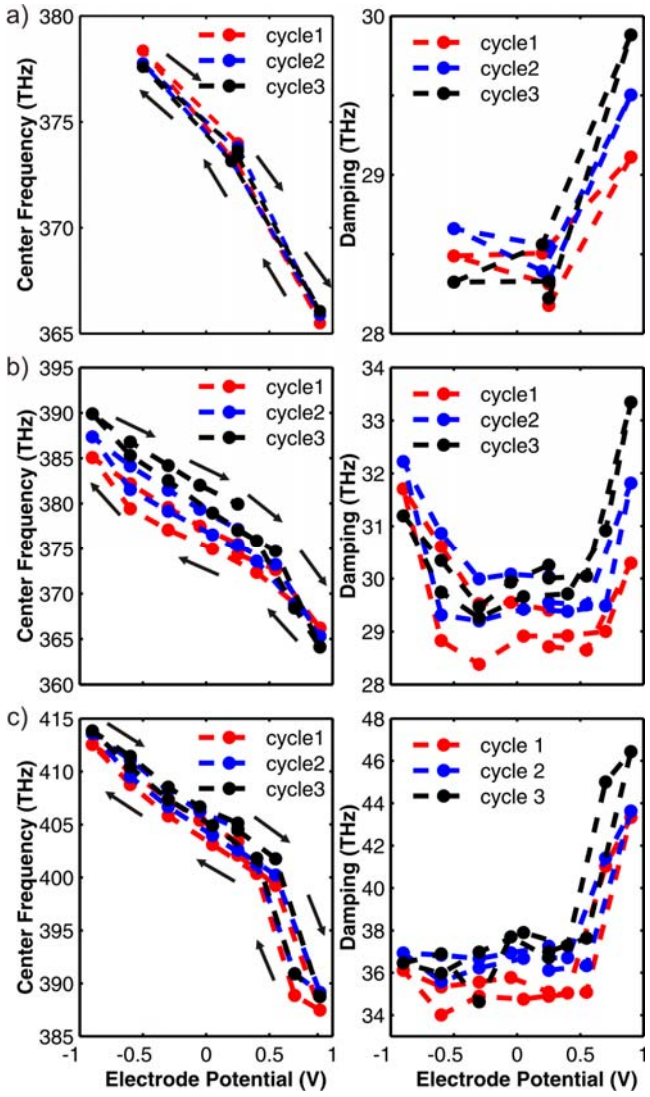

Fig. 5. Split-ring-resonator resonance positions (left-hand side colum) and dampings (right-hand side columns) as obtained from Lorentzian fits to the measured data as in Fig. 4 for three complete electrode-potential cycles in each sub-panel, a) - c). The gold film thickness is 10 nm. a) Electrode-potential window ranging from –0.5 V to + 0.9 V and immediately after the original N=10 training cycles. b) Following the measurements shown in a) and for a larger electrode-potential window ranging from –0.9 V to + 0.9V. c) Following b) and an additional 100 cycles, i.e., N=110. Note that, for the conditions of a) and c) very nearly reversible electrochemical modulation of the optical resonance positions is obtained.

To further test our overall interpretation, we have performed additional experiments in which the gold film thickness of the SRR is varied systematically. Clearly, we expect smaller reversible frequency shifts from surface-charge effects for thicker Au films due to the less favorable surface-to-volume ratio. Results of corresponding experiments are shown in Fig. 6. As expected, for a given voltage modulation within the reversible regime, the observed frequency swing decreases with increasing gold thickness d of the SRR, approximately proportional to $1/d$. Finally, the experimental observations are in qualitative agreement with simple numerical modeling where the

extra electronic charge in the space-charge layer at the metal side of the metal-electrolyte interface is modeled in terms of an extra layer of metal, increment the net number of conduction electrons in the structure.

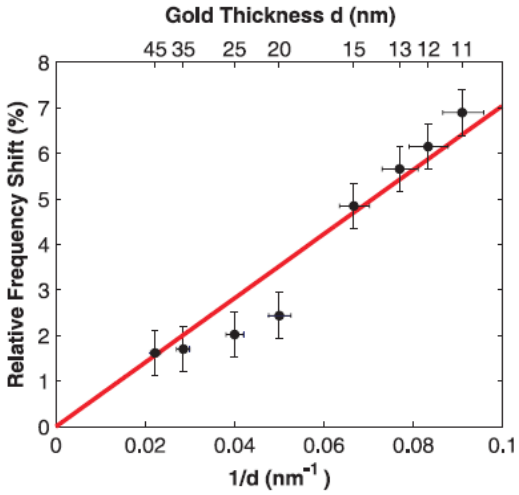

Fig. 6. Relative split-ring-resonator resonance frequency modulation (i.e., ratio of frequency shift and center frequency for zero electrode potential) as obtained from Lorentzian fits to the measured data as in Fig. 4 versus the inverse, $1/d$, of the gold thickness. In all cases, after the initial electrochemical training, the electrode-potential is varied in the range from –0.9 V to + 0.9 V following $N = 100$ electrochemical cycles. Obviously, the reversible modulation is more pronounced for thin gold structures due to their larger surface-to-volume ratio. The red graph is a straight line of best fit $\propto 1/d$.

References

- own work with complete titles -

[1] J. Weissmüller, R. N. Viswanath, D. Kramer, P. Zimmer, R. Wurschum, H. Gleiter, Science **300**, 312 (2003)

[2] H. -J. Jin, X. -L. Wang, S. Parida, K. Wang, M. Seo, J. Weißmüller, Nano Lett. **10**, 187 (2010)

[3] J. B. Pendry , A. J. Holden , D. J. Robbins , W. J. Stewart , IEEE Trans. Microwave Theory Tech. **47**, 2075 (1999)

[4] L.-H. Shao, M. Ruther, S. Linden, S. Essig, K. Busch, J. Weissmüller, and M. Wegener, ***Electrochemical Modulation of Photonic Metamaterials***, Adv. Mater. **22**, 5173 (2010)

[5] M. Ruther, L.-H. Shao, S. Linden, J. Weissmüller, and M. Wegener, ***Electrochemical restructuring of plasmonic metamaterials,*** Applied Physics Letters **98**, 1 (2011)

[6] S. Linden, C. Enkrich, M. Wegener, J. F. Zhou, T. Koschny, C. M. Soukoulis, Science **306**, 1351 (2004)

[7] M. Smetanin, R. N. Viswanath, D. Kramer, D. Beckmann, T. Koch, L. A. Kibler, D. M. Kolb, J. Weißmüller, Langmuir **24**, 8561 (2008)

[8] B. E. Conway, Prog. Surf. Sci. **49**, 331 (1995)

[9] M. H. Hölzle, V. Zwing, and D. M. Kolb, Electrochim. Acta **40**, 1237 (1995)

[10] M. A. Schneeweiss and D. M. Kolb, Solid State Ionics **94**, 171 (1997)

[11] G. Lippmann, Ann. Chim. Phys. **5**, 494 (1875)

[12] K. P. Chen , V. P. Drachev , J. D. Borneman , A. V. Kildishev , V. M. Shalaev , Nano Lett. **10**, 916 (2010)